Journal of The Electrochemical Society, **151** (11) A1961-A1968 (2004)
0013-4651/2004/151(11)/A1961/8/$7.00 © The Electrochemical Society, Inc.

Chromium Poisoning of LSM-YSZ SOFC Cathodes

I. Detailed Study of the Distribution of Chromium Species at a Porous, Single-Phase Cathode

S. C. Paulson* and V. I. Birss*,z

Department of Chemistry, University of Calgary, Calgary, Alberta T2N 1N4, Canada

Detailed chemical and surface structure analyses are presented for an 8 mol % yttria-stabilized zirconia (YSZ) wafer, partially covered with a thin, porous $(La_{0.8}Sr_{0.2})_{0.98}MnO_3$ (LSM) film electrode, after being cathodically poisoned in the presence of a chromia source at 800°C. Under the conditions used, the newly deposited Cr-containing compounds were distributed not only in and around the electroactive LSM-YSZ-air triple-phase boundary (TPB) interface region, but also extending *ca.* 500 μm from the edge of the LSM film onto the YSZ surface. The distribution and structure of the Cr species on the YSZ surface was directly correlated with variations in the cathodic polarization of the half-cell for a solid oxide fuel cell (SOFC). Such structuring was not anticipated, considering that the electrochemical activity is thought to occur only at the LSM-YSZ-air TPB. Evidence presented here suggests that Cr_2O_3 plays an important role in extending the electroactive LSM-YSZ-air TPB out onto the YSZ surface by effectively creating a new Cr_2O_3-YSZ-air TPB region.
 [DOI: 10.1149/1.1806392]

Manuscript received March 17, 2004. Available electronically October 27, 2004.

Loss of performance over the lifetime of operation is a major concern in the development of commercially viable, planar solid oxide fuel cell (SOFC) systems. In terms of Sr-doped lanthanum manganite (LSM) cathodes deposited on yttria-doped zirconia (YSZ), one primary suspected cause of long-term performance degradation is the accumulation of Cr species at and near the cathode-electrolyte interface. Numerous studies have shown that rapid cathode performance degradation occurs when chromia forming metal interconnects, typically Cr-containing steel alloys, are used in these cells, and that several types of Cr species are observed in regions where the cathode, electrolyte, and oxygen gas all come together at common locations.[1-12] Because this triple-phase boundary (TPB) is located hundreds or even thousands of micrometers away from the metal interconnect, it is generally recognized that the high oxygen environment of the cathode compartment leads to the formation of volatile Cr(VI) oxides and oxyhydroxides from the protective Cr_2O_3-containing film on the metal interconnect.[13] These species then diffuse throughout the cathode compartment where they can re-equilibrate to deposit solid Cr_2O_3. This would be expected to occur most readily in regions where there is a low oxygen partial pressure, a reducing environment, and the means to remove electrogenerated oxygen anions (O^{2-}). Because the highest rate of oxygen consumption occurs at the TPB of an active cathode, with concurrent production of oxygen anions, it would be logical to assume that the highest concentration of deposited Cr_2O_3 would be at the TPB. Not only would this reaction compete with the electrochemical reduction of oxygen, but it would also result in the deposition of solid species that could block further reduction of oxygen gas at these sites.

Research on this problem might have shifted away from basic mechanistic studies if it had not been for contradictory and unexplained observations reported in the literature. The first is that Cr-poisoning rates observed by Jiang *et al.*[6-8] and Matsuzaki *et al.*[4,5] were exceedingly rapid, on the order of hours for severe poisoning, rather than the weeks or months noted for some full cell studies.[14] The second is that certain combinations of cathode and electrolyte materials have been reported to resist Cr-poisoning effects, and that deposited Cr species are either lacking or different in composition than what is observed for the LSM-YSZ cathode system.[1-4] The third is that Cr-containing species have been observed to be deposited over the surface of the adjacent YSZ in bands that extended hundreds of micrometerss away from the LSM cathode, well beyond what has been identified as the LSM-YSZ-air TPB region.[6] This latter point implies that all YSZ-air interfaces near the TPB region, including those buried within porous single-phase or even composite LSM-YSZ cathodes, will be affected in a similar manner.

In this paper, experimental results are presented that address the third point, as well as theories on how the reactive LSM-YSZ-air TPB interface might be influenced by Cr species. Employing a porous LSM film on a YSZ substrate, a 17-4 stainless steel contact in nonflowing, ambient air at 800°C, and a −0.5 V applied potential, we have observed the rapid loss of cathode activity and concomitant formation of a Cr_2O_3 film on the surface of the YSZ substrate. The continuous band extended *ca.* 500 μm from the edge of the LSM film across the YSZ surface, and is composed of a series of concentric rings, the number of which mirrors the number of sequential electrochemical experiments applied to the sample. Other Cr-containing phases, such as $(Cr, Mn)_3O_4$ spinels, are also generated, but they are mainly restricted to the LSM surface, especially immediately next to the YSZ surface. To a lesser degree, they are also thinly scattered across the YSZ surface near the LSM. Finally, we offer an explanation for why Cr_2O_3 film growth extends out over the YSZ surface, while remaining consistent with traditional views on Cr-poisoning mechanisms. Subsequent papers in this series will address how varying the structure of the LSM-YSZ composite electrode, applied temperature to the cell, and composition of the metal electrical contact will influence the rate of Cr species deposition or removal, their chemical evolution to new species, and, ultimately, the resulting loss or recovery of the half-cell performance.[15]

Experimental

Samples of porous $(La_{0.8}Sr_{0.2})_{0.98}MnO_3$ (LSM, Praxair Ceramics Inc.) coated on densified 8 mol % Y_2O_3-ZrO_2 wafers (YSZ, Ceraflex) were prepared by Fuel Cell Energy, Inc. (formerly Global Thermoelectric, Inc.) in the unfired state. The *ca.* 15 μm thick LSM films on these wafers were prepared by suspending the LSM powder ($d_{50} \approx 0.5$ μm for the average particle size) as an organic-ceramic slurry and silk screening the mixture onto a 5 × 5 cm square wafer of 200 μm thick, densified YSZ (4 × 4 cm film area). For individual experiments, *ca.* 12 × 12 mm samples were cut from the modified wafer and portions of the LSM film were removed with a razorblade such that a *ca.* 4 × 4 mm square of LSM film rested on each sample. Samples were then fired at 1150°C for 2 h, with heating and cooling ramp rates of *ca.* 200°C/h at the higher temperature ranges.

For this particular study, Pt paste (Ferro Pt 4082, 74.3% Pt metal) was deposited at two locations on the back side of one 12 × 12 mm LSM-YSZ sample to effectively create the counter and reference electrodes (CE and RE). The CE was located on the YSZ directly

* Electrochemical Society Active Member.
z E-mail: birss@ucalgary.ca

across from the LSM film and covered an area of roughly 0.5 cm^2. The RE was located closer to the edge of the LSM-YSZ sample and covered an area of about half that of the CE. The Pt paste was sintered by placing the entire sample in a furnace and heating at 1000°C for *ca.* 1 h.

For the electrochemical studies, a specially designed electrochemical cell was employed, in which the LSM-YSZ sample and various contacts were sandwiched between 19 mm diam ceramic disks (contact surfaces grooved with 1 mm deep gas diffusion channels) and held in place by a spring-loaded Ni wire. The cell was open to ambient, quiescent air. Extreme care was not exercised in controlling the water content of the air entering the cell. However, the ambient air humidity was *ca.* 1 mol % during the time period of the study. The CE and RE contacts each consisted of a 100 mesh Pt gauze (spot-welded to 0.37 mm diam Pt wires), contacted with fresh Pt paste to the sintered Pt locations. The working electrode (WE) contact consisted of a 6.3 mm diam 17-4 PH stainless steel (SS) disk (15.21% Cr, 4.57% Ni, 3.16% Cu, 0.85% Mn, 0.40% Si, 0.25% Nb, 0.08% Mo, 0.031% C, 0.028% N, 0.020% Al, 0.018% P, 0.001% S), machined to a point on one face such that the steel point only contacted the LSM surface. The gap between the majority of the steel surface and the LSM-YSZ ceramic surface was ca. 0.5 mm. The steel was not preconditioned prior to use. The backside of the steel was contacted to Pt gauze with Pt paste. A spring-loaded quartz rod was used to apply very light pressure to the 17-4 SS/LSM contact.

The electrochemistry was carried out using a computer controlled, EG&G 173 potentiostat/276 interface module that was programmed to perform a series of experiments that alternated between five consecutive cyclic voltammogram (CV) scans (5 mV/s) between −0.5 and 0.1 V *vs.* Pt/air, and a 19,900 s (*ca.* 5.5 h) chronoamperometry experiment at −0.5 V. Scanning electron microscope (SEM) images were acquired using a Philips/FEI ESEM under high vacuum using a 15 kV excitation voltage. A JEOL JXA-8200 electron microprobe was used to generate wavelength-dispersive X-ray spectroscopic (WDX) maps using either a 10 or 15 kV excitation voltage. Samples were vapor-coated with carbon prior to initial imaging. Higher resolution SEMs required removing the carbon film by heating the sample at 600°C for 2 h in air, and then coating the sample with a sputtered film of 1:1 Pd:Au. For the images presented in this paper, it should be noted that the orientation of the sample sometimes changes from figure to figure.

Results and Discussion

From our work, all samples composed of a porous LSM film coated onto a dense YSZ substrate show extreme symptoms of Cr-poisoning when cathodically polarized at 800°C in the presence of a 17-4 stainless steel electrical contact and air. When a fixed potential is applied, poisoning is observed as a rapid decrease in current output with time over a period of 5 to 10 h. After this phase, the current tends to stabilize at a much lower magnitude, often 20 to 100 times lower than the initial currents. The rate at which a sample is poisoned, and the degree to which that sample is poisoned, varies greatly, and is dependent on a number of factors, including gas flow rate, oxygen and water content, gas flow restrictions around and throughout the cathode, the type of metal interconnect employed, and local temperatures. Such studies are outside of the scope of the present paper, and will instead be addressed in the following papers.[15] Here, we present results for the full characterization of one sample generated under a particular set of controlled conditions.

Electrochemical study.—Figure 1 shows the overall decay of the O_2 reduction current with time at −0.5 V *vs.* Pt/air. Initially, and subsequently every 5.5 h thereafter, the experiment was interrupted by five CV scans, with the final scan in each case shown in the inset of Fig. 1. The entire study was run in ambient, quiescent air at a furnace temperature of 800°C, using a 17-4 SS point contact. As can be seen in the main portion of Fig. 1, the current rapidly decayed during the first 5 h of the experiment, and then stabilized for the remaining 40 h. The eight CVs (Fig. 1, inset) all exhibit an underlying linear I/E response, as expected for a resistive system based on a thick YSZ electrolyte, but otherwise follow the same trend observed for the fixed potential studies. The magnitude of the current at all potentials was highest in the first CV, and then decayed to and stabilized at a new level for all of the remaining CVs. Although difficult to discern in the inset in Fig. 1, an electrochemical characteristic unique at 800°C to a Cr-poisoned LSM-YSZ sample is the presence of a new cathodic redox wave between *ca.* −0.15 and −0.3 V. Possible explanations for this wave are presented in Ref. 15. Note that the magnitude of the current decay shown in Fig. 1 is not as extreme as typically observed for other samples that are polarized under similar conditions at −0.5 V from the very start of the experiment. For this sample, the initial decay occurred during the initial series of 5 CV scans.

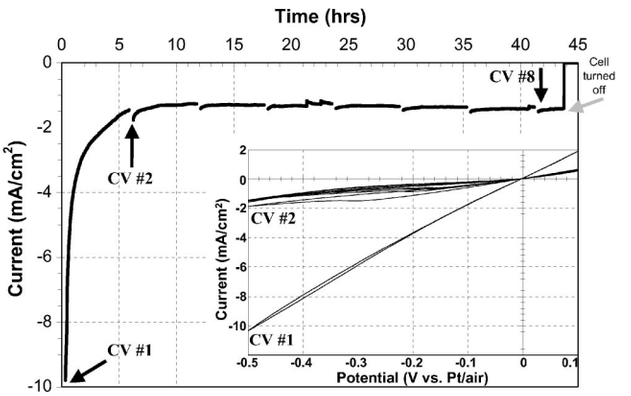

Figure 1. 800°C electrochemical study of the LSM-YSZ sample in quiescent room air where a 17-4 stainless steel point contact was used as the current collector. The single, continuous study consisted of 5 CVs between 0.1 and −0.5 V at 5 mV/s, followed by −0.5 V applied over *ca.* 5.5 h. This combination was repeated 8 times. The main figure shows the I *vs.* V curve for the −0.5 V constant potential study, and the inset shows the 8 CVs (last cycle shown for each set of 5 taken) run at the same time. Note that the furnace temperature ramp-down from 800°C was initiated *ca.* 2 h after the electrochemical study was terminated.

Characterization of the YSZ surface species.—After the electrochemical study was completed and the cell disassembled, the ceramic sample was carbon-coated and then thoroughly characterized by SEM and electron microprobe analyses. This sample had some of the highest surface concentrations of Cr species of any of our LSM-YSZ samples studied thus far. In fact, a faint green band on the YSZ surface around the edge of the LSM film could be observed visually. It is not exactly clear at this point as to which conditions led to this heavy deposition, although certainly the use of stagnant room air, 800°C temperature, and the very close proximity of the SS contact to the ceramic surface greatly assisted the process. Jiang *et al.* have shown that the location and composition of the Cr-containing deposits are highly dependent on the air flow rate.[8] Certainly the conditions employed in this study were conducive for the liberation of volatile chromium oxide species, considering that the high temperature, corrosive air environment led to the formation of a thick, black oxide film on the surface of the 17-4 SS point contact.

Figure 2 shows the SEM secondary electron (SE) and backscattered electron (BSE) images of one corner of the square LSM film after being Cr-poisoned via the electrochemical experiment shown in Fig. 1. Although not readily seen in the SE image, a *ca.* 500 μm wide band that resides on the YSZ surface and surrounds the LSM film is clearly defined in the BSE image. Furthermore, seven rings can be seen within this band when examined at a higher resolution (see Fig. 4 below). When the outer edge of the band is included, a total of eight rings exist. Similar observations have been made by Jiang *et al.*, although rings within the band have only been observed when the Cr-containing stainless steel is in very close contact with the ceramic surface, and when nonflowing, stagnant air is used.[8] In

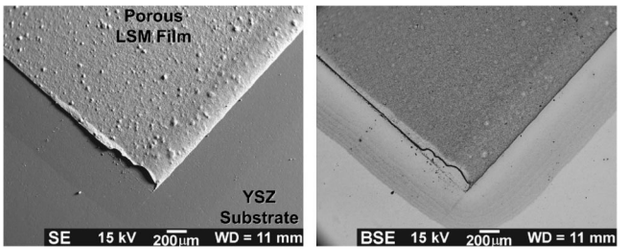

Figure 2. SEM SE and BSE images of one corner of the LSM cathode after electrochemically Cr-poisoning the LSM-YSZ sample (see Fig. 1). Note that the jagged edge on the left LSM edge was created when a razorblade was used to remove excess LSM prior to sintering at 1150°C. As a consequence, high image contrast due to high surface relief is seen along the LSM edge in the BSE image.

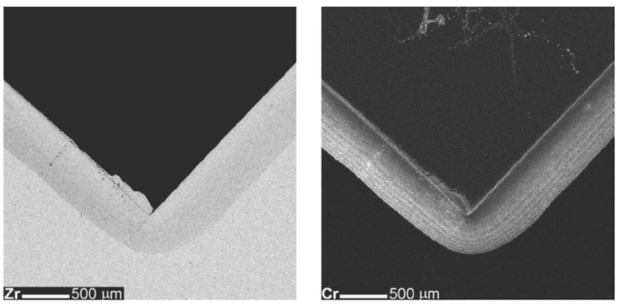

Figure 3. WDX Zr and Cr element maps of the same region shown in Fig. 2 (10 kV excitation voltage, 20 ms dwell time per pixel.)

addition, we have not observed this band on LSM-YSZ samples that were exposed to the same conditions as in Fig. 1, but were left unpolarized. This point is made even more apparent in parallel studies by our group where two LSM films are placed side-by-side (*ca.* 700 μm apart) on the same YSZ substrate. Only the LSM film that is contacted and polarized as the working electrode will develop a Cr band around it. Because the conditions for the air gap between the bulk portion of the stainless steel and both LSM films were the same (excluding the point of contact), we concluded that both LSM films were exposed to the same concentration of volatile Cr(VI) species. Thus, as noted by other researchers,[6,8] cathodic polarization in the presence of a chromia source is a prerequisite for the formation of this band.

The band and rings are not necessarily uniformly distributed around the perimeter of the LSM film. From BSE images of the entire sample surface (not shown), we found that the intensities and shapes of the band and rings vary from one side of the LSM film to the other. Jiang *et al.* found that the band and rings preferentially grew out from the LSM film perimeter around points along a 3 mol % YSZ surface that had an exceedingly restricted air gap between the surface and the chromia source.[8] The implication is that higher concentrations of gas-phase Cr species reside in these more restricted regions, and thus more would be available for conversion to solid phases. In our case, variations in the height between the surface of the ceramic sample and the 17-4 SS electrical contact likely existed, leading to the observation of a darker and broader band off of one side of the LSM film relative to the other.

Also, because the formation of the band and rings is cathodically driven, an asymmetric alignment of the working and counter electrodes (*i.e.*, an uneven distribution of the potential across the electrolyte) might also lead to nonuniform deposition of new surface species. We have also observed that the presence of isolated LSM particles on the YSZ surface strongly influences the shape of this band. Although not readily noticeable in Fig. 2, other regions and other samples have shown extreme cases where the band will extend out from what would otherwise be electronically isolated patches of LSM, in much the same way that it does from the electrically contacted LSM. The net effect is that the outer edge of the band will often contain ripples, waves, and large rounded features that correspond to LSM debris on the YSZ surface.

To identify the chemical composition of this band, the sample surface was mapped via WDX spectroscopy for relative concentrations of Zr, Cr, La, Mn, and Sr. Figure 3 shows the resulting maps for Zr and Cr. It can be seen that the band/rings in the BSE image are composed of high concentrations of Cr species, and that these species occur as a thin film on top of the YSZ. [The maximum escape depth of X-rays for WDX detection was calculated by Monte Carlo modeling software (Electron Flight Simulator, version 3.1-E) to be roughly 0.5 μm for 10 keV excitation of YSZ with a density of 5.95 g/cm^3. Because Zr can be readily observed in the band region, qualitatively speaking, the Cr-containing material in the band is well under a micrometer in thickness.] At the same time, the Mn map (not shown) does not show concentrations of Mn above background in the Cr band region, except along the LSM film perimeter and, to a far lesser degree, in scattered, isolated, micrometer-sized sites throughout the band region. General variations in the concentration of Cr in the band are also noticeable, with higher concentrations further away from the edge of the LSM and in a narrow region along the LSM film perimeter. There also exist some "Cr" markings on the LSM surface that correspond to where the point of the 17-4 SS contact scraped across the surface during cell assembly and ultimately came to rest.

Semi-quantitative WDX spot element analyses of the YSZ surface were performed to ascertain the magnitude of the variation in the concentration of Cr species across the band. If the Cr species in this region are limited to one type of compound, and the density of this compound does not vary significantly across the surface, then this information would give the relative concentration of that compound. Because EDX and WDX spot analyses in the Cr-containing band region only show Cr and elements associated with YSZ, and little, if any, Mn, it would be logical to assume that the Cr species are composed of Cr_2O_3, by far the most stable oxide of chromium under the conditions employed here.[16]

Figure 4a shows a plot of calculated mass percentage of a given metal oxide, based on metal oxide standards run immediately prior to the analyses, versus the location of each spot analysis relative to the LSM edge. Figure 4b shows the locations where each spot analysis was carried out relative to a BSE image of the Cr-band. Figure 4b also more clearly defines the band edge and the seven rings found within the Cr band, with the exception of the first band, which is not seen in Fig. 4b, but was observed at other locations on the sample.

The mass percentages given in Fig. 4a are fairly reliable, in that the totals account for greater than 94% of the calibrated intensities (which do not include the 1-3% HfO_2 that exists in the YSZ) and come fairly close to the anticipated 13.8 mass % Y_2O_3 and 82.2 mass % ZrO_2 for commercial 8 mol % YSZ. Figure 4a clearly shows that the concentration, or more precisely the average thickness of the Cr_2O_3 film, more than doubles from the LSM film perimeter out to the band edge, dropping to zero beyond the band region. In general, the ZrO_2 content inversely mirrors this trend, as expected, although numerous local inconsistencies do exist, especially near the LSM film perimeter, where shadowing of the sample for certain detector locations becomes an issue.

Various morphologies are observed for the Cr_2O_3 film. Further out from the LSM film perimeter, crystal platelets are observed, as seen in the SEM images in Fig. 5a and b. Jiang *et al.* observed similar crystals, and attributed them to Cr_2O_3.[8] The two circles (○) in Fig. 4b denote where the SEMs in Fig. 5 were taken and correspond to a ring region (Fig. 5a) and the band edge (Fig. 5b). Although the SEMs show that the Cr_2O_3 film is rough, crystalline, and highly irregular in thickness, it is not known at this point whether the Cr_2O_3 film is continuous, and as a consequence, whether or not it completely blocks oxygen transport to the YSZ surface.

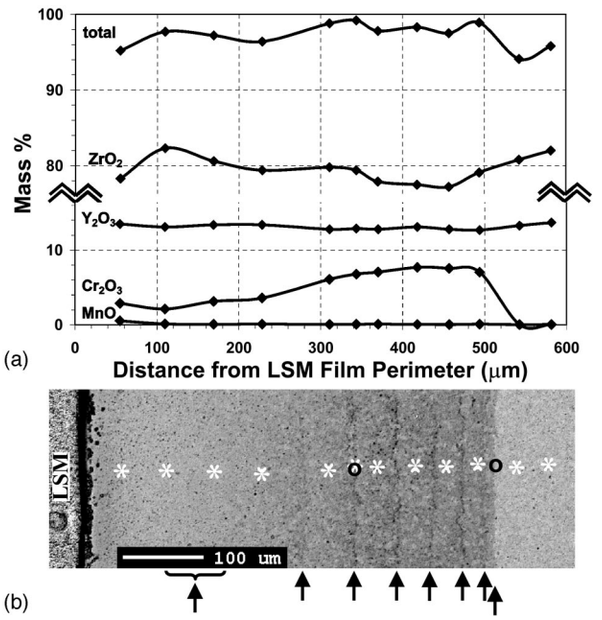

Figure 4. (a) Semi-quantitative WDX spot element analyses of the YSZ surface *vs.* distance from the LSM edge. (5 μm spot size, 15 keV, 30 nA, ZAF routine using mineral standards.) Diamonds denote the location of each spot analysis. Note that *ca.* 1-3% HfO_2 was not included in the mass % calculations. (b) BSE image (located at lower left portion of Cr-film in Fig. 2 and 3) showing where the corresponding spot analyses were taken (*), along with arrows pointing out the locations of each bandedge. The two circles (O) denote where the SEM images in Fig. 5 were taken. Note that the dark border along the jagged LSM film edge is due to shadowing.

On the YSZ surface, but closer to the LSM film perimeter, another Cr_2O_3 structure is observed, as well as a significant number of diamond-shaped, octahedral spinel crystals. A particular zone (outside the viewing area of Fig. 2) is shown in the SEM image in Fig. 6a. This area was chosen because the height variations between the LSM and YSZ surfaces were not as dramatic as that seen in Fig. 2, so shadowing effects were less pronounced. In Fig. 6a, and in the higher magnification image seen in Fig. 6d, nodular features (~60 nm diam) are seen. These features completely cover the YSZ surface (see the lower left corner of Fig. 5b for comparison with an unaltered YSZ surface), and are occasionally interspersed with octahedral spinel crystals (bright features on the YSZ surface in Fig. 6a). The nodular features were also observed by Jiang *et al.* and ascribed to Cr_2O_3.[8]

Detailed WDX element spot analyses clearly show that the isolated spinel crystal on the YSZ surface are composed only of Cr, Mn, and associated Y, Zr, and Hf. Other researchers have identified these crystals as the $(Cr, Mn)_3O_4$ spinel phase,[6,8,11,12] and our evidence supports this claim. For instance, Fig. 6b and c show the WDX Cr and Mn element maps for the same area shown in Fig. 6a. The Cr map shows a relatively even distribution of Cr on the YSZ surface, except where the spinel crystals exist. The higher Cr concentrations in these locations reflect the fact that the spinel crystals extend above the Cr_2O_3 film surface, and thus are probably much thicker than the Cr_2O_3 film. Although concentrations of Mn across the YSZ surface were found to be at, or just above, background levels for the conditions and WDX detector employed, the corresponding Mn map does show that relative concentrations of Mn follow those of Cr in the Cr map. Thus, greater than trace amounts of Mn are associated with Cr and the spinel crystals on the YSZ surface. Evidence in the literature suggests that, at temperatures similar to those employed in this study, and at low relative concentrations of Mn to Cr, the $MnCr_2O_4$ spinel phase is in equilibrium with Cr_2O_3 and Mn-doped Cr_2O_3.[16,17]

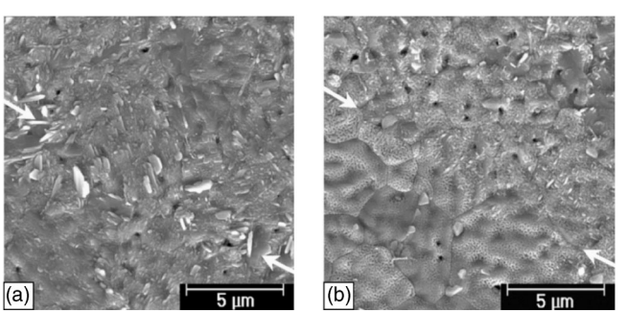

Figure 5. Higher magnification SE images taken of a ring (a) and the bandedge (b) (see circle locations in Fig. 4). The arrows point out the general orientation of the roughly 5 μm wide ring, and the bandedge. Note that both pictures have the same general orientation as the SE and BSE images in Fig. 2. Sample coated with 1:1 Au:Pd.

Origin of the Cr band.—One of the major questions to arise relates to how a continuous Cr band, with regular substructures and extending hundreds of microns from the LSM-YSZ TPB, could form on the surface of an otherwise electronically insulating YSZ substrate, and why its growth is apparently electrochemically driven. Independent of any electrochemical process, Cr(VI) oxides in the vapor phase can contribute to the formation of crystalline Cr_2O_3 films via the fully reversible reaction shown in Eq. 1 [$Cr(OH)_2O_2$ is the most prevalent volatile Cr species in humid air at 800°C.][13,18]

$$2Cr(OH)_2O_2(g) = Cr_2O_3(s) + 3/2O_2(g) + 2H_2O(g)$$

$$K_{eq} = 1.5 \times 10^4 \quad \text{at } 800°C \qquad [1]$$

However, this would be limited to the random growth of crystals, rather than a continuous band clearly emanating from the LSM-YSZ interface, as nucleation sites would be expected to be randomly distributed across the YSZ surface.

In terms of electrochemically driven processes, O_2 reduction occurs only at the LSM-YSZ-air TPB prior to exposure to a chromia source, and there is every reason to believe that the cathodic reactions will continue to occur at this TPB after Cr poisoning. It can be easily argued that Cr(VI) species, such as $Cr(OH)_2O_2$, are reduced at all LSM-YSZ-air interfaces, including at the LSM film perimeter, to form Cr_2O_3 and oxygen anions (O^{2-}), as proposed by others and shown in Eq. 2[11-13]

$$2Cr(OH)_2O_2(g) + 6e^- = Cr_2O_3(s) + 3\ O^{2-} + 2H_2O \qquad [2]$$

The amorphous Cr_2O_3 deposit would then slowly reorganize to form Cr_2O_3 crystals as it re-equilibrates with the gaseous environment.

Beyond the LSM film perimeter, a new TPB must form to propagate a continuous Cr_2O_3 film across the open YSZ surface. We propose that, due to the reasonable high-temperature electronic conductivity of Cr_2O_3 (0.2 to 0.02 S/cm at 800°C[19]), a new kind of TPB, composed of Cr_2O_3-YSZ-air, is formed. This interface would then form the basis of the propagation zone that, along with the high ionic conductivity of YSZ, allows the electrochemical growth of a more or less continuous Cr_2O_3 film across the YSZ surface. Because this process is cathodically driven, in much the same way that it was driven at the LSM-YSZ-air TPB region, the structure of the Cr_2O_3 film in the band region would be influenced by the polarization history of the sample. Using this logic, more rapid Cr_2O_3 film growth would occur at more cathodic polarization potentials, slowing when the polarization is decreased and stopping when the polarization is removed. At the same time, electrochemical deposition of

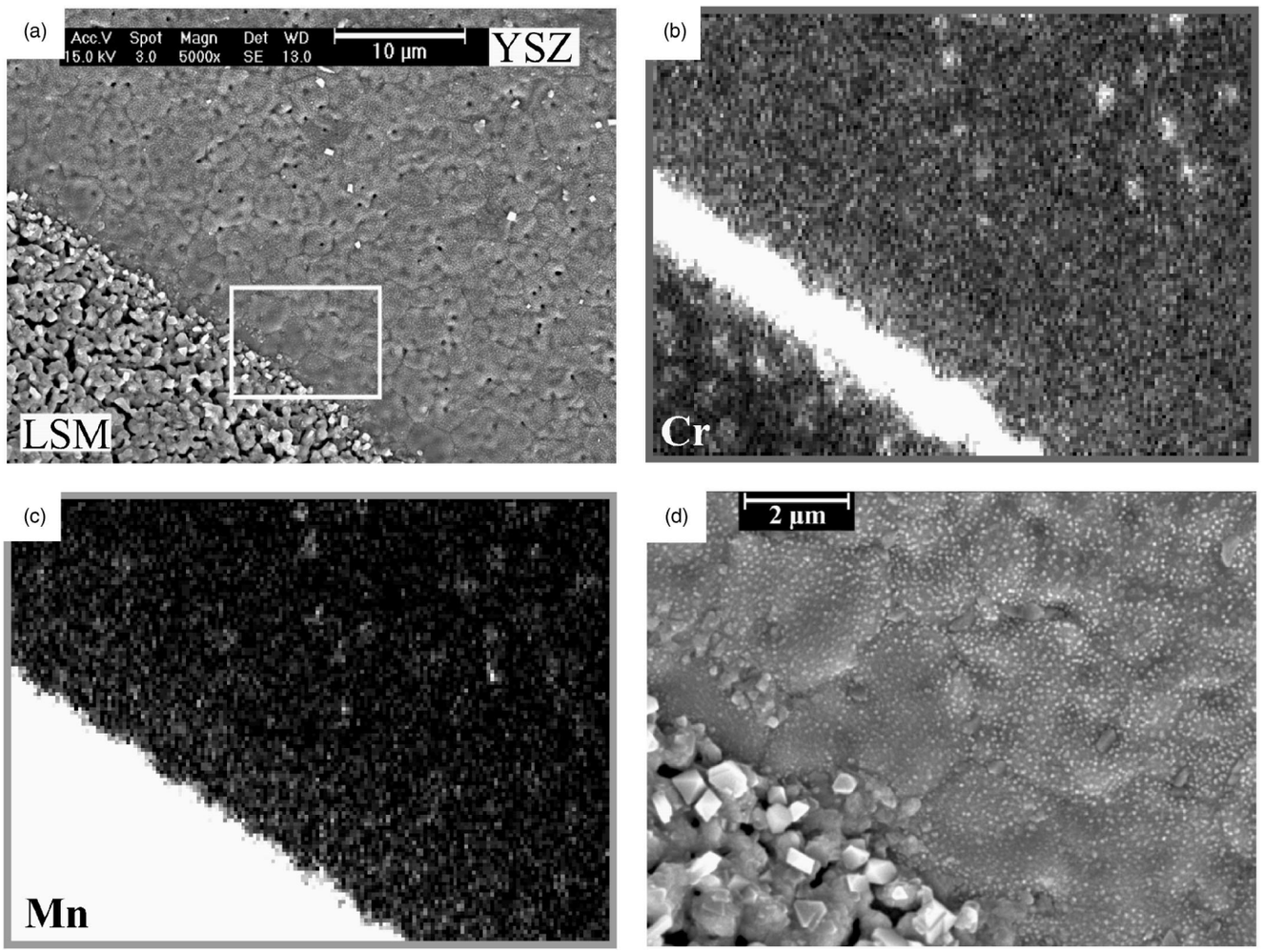

Figure 6. (a) High magnification SE image taken of the LSM film perimeter (original screen-printed edge located outside the viewing area in Fig. 2). Sample coated with 1:1 Au:Pd. (b and c) WDX Cr and Mn element maps of the same area as (a). (Carbon coated, 15 kV, 20 ms dwell time per pixel. High contrast images used to emphasize differences found on the YSZ surface.) (d) SE image taken in the boxed region in (a). Note that each map and image has a similar orientation to that found in Fig. 2.

Cr_2O_3 is in dynamic competition with the gas-phase equilibration f Cr_2O_3 with $Cr(OH)_2O_2$ (Eq. 1) In addition, because the Cr_2O_3-YSZ-air interface is extended away from the vastly more electronically conductive LSM cathode as the Cr_2O_3 film grows, it would be expected that the increasing Cr_2O_3 film resistivity would become more of a factor the further the Cr_2O_3 bandedge is from the LSM film perimeter. This would effectively slow Cr_2O_3 film growth on the outer portions of the band and ultimately limit the extent of film growth across the YSZ surface.

All of these factors would contribute to the band features observed in Fig. 4b. During the first extended period of polarization at −0.5 V, film growth would be rapid as amorphous and finely divided, crystalline Cr_2O_3 particles effectively extend the electronic conductivity of the working electrode beyond the LSM film out over the YSZ surface. During the second set of five CVs, the less negative polarization potentials (relative to −0.5 V) would lead to considerably slower film growth, such that film reorganization and crystal growth (Eq. 1) become more important. With each subsequent period of −0.5 V polarization, the Cr_2O_3 film would continue to grow at the new TPB, albeit at a slower rate because of the larger voltage drop across the increasingly wider film band. This would explain why the rings become more closely spaced and the interjacent Cr_2O_3 film becomes more dense the further it is located from the LSM film perimeter. Likewise, as polarization induced film growth slows down, Cr_2O_3 re-volatilization and crystal growth become more dominant, which is why larger Cr_2O_3 crystals (observed in Fig. 5) are found in regions further away from the LSM film perimeter. If the leading edge of the Cr_2O_3 band were to reach more electronically conductive, but otherwise isolated, LSM particles on the YSZ surface, Cr_2O_3 film growth will occur on all edges of the LSM particles because they simply extend the TPB region once electrically contacted by the Cr_2O_3 film. Although not seen in the sample studied here, it is anticipated that film growth would eventually subside as the potential at the Cr_2O_3-YSZ-air interface drops below that necessary to drive Cr(VI) reduction to Cr_2O_3.

From all indications, the well-defined rings in the Cr_2O_3 band formed during the CV portion of the electrochemical study, but there remains a question as to why the CV experiments cause their formation. The lower average applied potential (*vs.* −0.5 V) during each set of CV cycles would result in slower Cr_2O_3 film growth and probably a more dense film. The high degree of crystallinity of the Cr_2O_3 in the rings (see Fig. 5a) would suggest that, during pauses in film growth, rapid crystal formation occurs preferentially at the leading edge of the band. This would occur if, during this time period, there existed a larger vapor-phase concentration of Cr(VI) species at the Cr_2O_3-YSZ-air TPB as a result of extensive re-volatilization of

Cr_2O_3. This phase shift would be enhanced if the reaction shown in Eq. 2 could be driven in reverse at the Cr_2O_3-YSZ-air TPB, *i.e.*, by anodically polarizing the electrode at +0.1 V during the CVs. However, attempts at cleaning Cr-poisoned surfaces using anodic polarization at +0.1 V have not been successful, and indeed, Jiang *et al.* noted that anodic polarization at higher potentials in the presence of a chromia source still led to Cr species deposition on the YSZ surface.[6]

Questions also remain as to how the Mn found in the spinel crystals migrated from the LSM onto the YSZ surface. Mn cations are known to have a limited solubility[20] and diffusivity[21] in YSZ at elevated temperatures, and our own work has shown that a large purple halo will form throughout YSZ adjacent to LSM when a composite LSM-YSZ sample is sintered at 1350°C. Certainly, a limited amount of Mn cation diffusion from Mn-excess LSM into the YSZ matrix would be expected at 1150°C. However, Jiang *et al.*[6] have observed extensive formation of $(Cr, Mn)_3O_4$ spinel crystals on the YSZ surface after polarization at 900°C. Presumably, the amount of Mn in these crystals is in excess of what would be supplied by residual concentrations of Mn cations in the YSZ matrix left over from prior sintering steps. Thus, it was argued that spinel formation resulted from polarization-induced migration of Mn^{2+} into and throughout the YSZ, and then subsequent reaction of Mn(II) species with the gaseous Cr(VI) species.[6]

In other studies, we have observed high densities of spinel crystals on YSZ within a zone extending tens of micrometers from the LSM film perimeter. In addition, during 600+h at 800°C, when attempts were made to thermally remove Cr species and then test the cathode behavior using a non-chromia-containing Pt working electrode contact, a portion of the Cr_2O_3-dominant band can be converted into one dominated by $(Cr, Mn)_3O_4$ spinel crystals. Differences seen here as compared to other researchers work probably result from the lower current densities used in our studies. Given more time and/or higher current densities, a significant mobility of Mn^{2+} cations may exist, in part because high local current densities might lead to high local temperature gradients and more rapid local diffusion/migration rates.

Characterization of species found on the LSM surface and below.—For samples composed of a porous film of pure LSM on a dense YSZ substrate, most of the active TPB lies at the buried LSM-YSZ interface, the composition of which is difficult to establish due to partial disruption of its structure during sample preparation. However, the LSM-YSZ-air TPB at the LSM film perimeter can be viewed as an approximate model of the buried LSM-YSZ-air interfaces. In Fig. 6a and d, it can be seen that, at the LSM film perimeter, and most noticeably on the surface of the LSM next to the perimeter, many distinctively shaped spinel crystals can be found. They are not only loosely associated with the LSM surface, but are also found within the crevices and as an integral part of the surface of what otherwise would be amorphous-looking LSM particles. Likewise, the highest concentration of Cr in the WDX element map in Fig. 6b is found at the LSM film perimeter, and specifically, on the LSM film. The $(Cr, Mn)_3O_4$ spinel crystals seen on the LSM film at the perimeter in Fig. 6d probably account for much of the observed Cr, although SEM and WDX studies have not given us conclusive evidence that Cr_2O_3 is missing from this zone. These observations are similar to our results obtained from solid-state reaction studies at 1150°C between intimately mixed LSM and Cr_2O_3 powders. SEM images show that an abundance of spinel crystals form only on top of LSM particles, rather than on the Cr_2O_3 particles or YSZ substrate surface.

The high concentrations of Cr seen at the LSM film perimeter in Fig. 6b do not extend across the outer surface of the LSM film, and instead, the Cr content decreases abruptly to levels well below that found on the adjacent YSZ surface. Beneath the LSM film, however, high concentrations of Cr species are observed. For other Cr-poisoned samples, when the LSM film was subsequently broken away from the YSZ surface, concentrations of Cr beneath the LSM tended to be relatively high and evenly distributed out to the original LSM film perimeter.

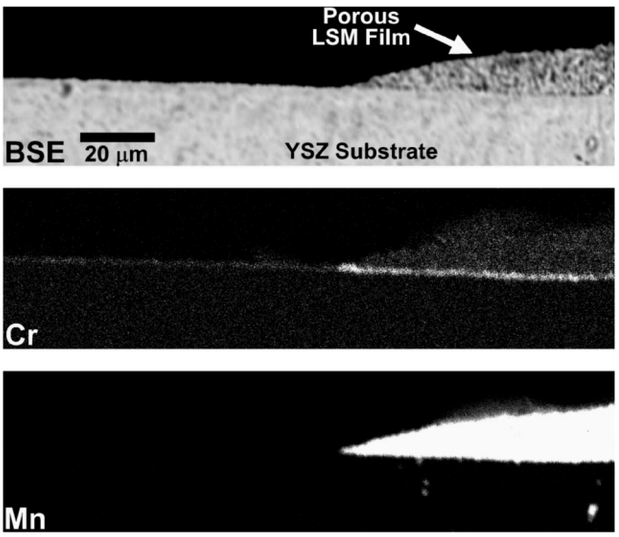

Figure 7. SEM BSE image and WDX Cr and Mn maps of a broken cross-section that includes the LSM film perimeter, Cr_2O_3 film, and a portion of the YSZ electrolyte. The region is offset by *ca.* 0.5 mm from that observed in Fig. 6. (Carbon coated, 15 kV, 25 ms dwell time per pixel.)

In Fig. 7, a cross-sectional SEM BSE view and corresponding WDX Cr and Mn element maps of the sample used in this study show that high concentrations of Cr species can be found along vast portions of the LSM-YSZ interface, as has been reported by other groups.[4,11,12] Although more difficult to see, the highest Cr concentration is found around the LSM film perimeter, and lesser amounts of Cr species are observed at the YSZ-air interface. High-resolution SEMs of the same interface (10,000 times magnification) did not show any direct evidence that the pores in the LSM near the underlying YSZ surface had been reduced in size or blocked by Cr species. Thus, we believe that the compounds responsible for the high Cr concentrations observed at the LSM-YSZ interface must be part of a very thin film that is well under 100 nm in thickness.

Implications for the electrocatalytic behavior of the LSM-YSZ interface.—Many of the physical observations presented above do not directly address the critical TPB regions beneath the LSM film where the majority of the electrochemical reactions occur. Certainly, the Cr_2O_3-dominant band observed in Fig. 3 and 4 would not directly contribute to Cr-poisoning effects, as the oxygen reduction activity of an LSM cathode is restricted to the LSM-YSZ-air TPB region, an area that is theorized to extend from tens of nanometers up to a micrometer around the point where the LSM simultaneously contacts the YSZ and air.[22-24] However, this band is symptomatic of what is likely to be occurring on the YSZ surface within the restricted confines of the porous LSM matrix. In addition, the band acts as a Cr species reservoir which readily maintains the vapor pressure of the Cr(VI) species in the gas phase.

Likewise, although a portion of the LSM at the LSM film perimeter becomes chemically converted to the $(Cr, Mn)_3O_4$ spinel phase, this is not definitive proof that LSM at all TPB regions has been similarly altered, or even that chemically converted LSM is responsible for the observed Cr-poisoning effects. What we can conclude at this time is that high concentrations of Cr are found around the LSM-YSZ interface, as seen in Fig. 7, that some of these Cr species are responsible for Cr-poisoning effects, and that an electrochemically driven reaction is responsible for the observed distribution of Cr species.

Interestingly, the highest concentrations of Cr are not found at the buried LSM-YSZ interface, but rather at the LSM film perimeter

(Fig. 7). A simple explanation for this observation is that concentrations of volatile Cr(VI) species are higher around the LSM film perimeter than within the LSM film. It is also possible that the TPB at the LSM film perimeter is slightly different in composition/structure from that at the buried interface, resulting in a higher cathodic activity (at least for Cr(VI) species reduction) in the former location.

Our observations from solid-state reaction studies between LSM and Cr_2O_3 have shown that $(Cr, Mn)_3O_4$ spinel phases do not form at 800°C, and instead, require temperatures greater than 1000°C, at which they preferentially form only on the LSM particles. A proposed reaction was given by Badwal *et al.* as $3CrO_3 + 3La_{0.8}Sr_{0.2}MnO_3 = 3La_{0.8}Sr_{0.2}Mn_yCr_{1-y}O_3 + (Cr_yMn_{1-y})_3O_4 + 2.5O_2$.[11] That we do observe spinel crystals on samples electrochemically polarized at 800°C, but only in certain zones along the LSM film perimeter, and only under cathodic polarization, strongly supports the notion that the formation of these crystals is related to the electrochemistry. Our observations also indicate that the above reaction must be modified in terms of an electrochemical reduction step that includes the formation and removal of O^{2-} anions.

Why the spinel crystals would form on the LSM particles many micrometers away from the LSM-YSZ-air TPB is less clear. Jiang *et al.* rationalized the formation of the spinel crystals on LSM as the direct reaction of electrochemically reduced Mn^{2+} cations with the volatile Cr(VI) species.[6] The presence of such cations so far away from the TPB requires either that they migrate out from the TPB, where they were originally generated, or that they are generated locally, with O^{2-} anions simultaneously migrating over great distances to the TPB. In any case, the observations presented above would suggest that all electroactive surfaces throughout the porous LSM film, whether they be located on the LSM or YSZ surfaces, are a target for reaction by the volatile Cr(VI) species, and that removal of electrogenerated O^{2-} anions can occur well outside of the region traditionally viewed as the TPB.

Conclusions

SOFC cathodes composed of LSM on a YSZ electrolyte are susceptible to performance degradation in the presence of chromia forming stainless steels, the preferred structural/interconnect material for planar cell designs. Although it is generally understood that cathodic deposition of solid, Cr-containing species at the LSM-YSZ-air TPB is a readily observable sign that performance degradation has occurred, the exact chemical and electrochemical reactions that are responsible for the various deposited Cr species observed largely remain unknown. Employing a half-cell design, in which a porous LSM cathode film occupies only a small portion of the YSZ electrolyte surface, we show that variations in the potential bias (between −0.5 and 0.1 V *vs.* Pt/air using a 17-4 stainless steel contact) at 800°C in stagnant air produce systematic variations in the location and density of certain Cr species on the LSM and YSZ surfaces.

On the YSZ surface, a film of crystalline and semicrystalline Cr_2O_3 was found to extend ~500 μm out from the LSM film perimeter, and contained repeating structural features in the form of thicker zones, or rings of Cr_2O_3. The eight rings observed exactly match the eight times the cathodic bias to the LSM was switched between an extended, −0.5 V constant potential bias, and a set of five potential cycles between −0.5 and 0.1 V. It is argued that the growth of such a film must initiate at the electroactive LSM-YSZ-air interface, and then propagate at a new TPB established by Cr_2O_3 as the cathode, YSZ as the electrolyte, and air as the volatile species transport medium. This Cr_2O_3-YSZ-air TPB, defined as the leading edge of the observed Cr_2O_3 band, allows the electrochemical reduction of Cr(VI) species and removal of O^{2-} anions. Furthermore, the growth and structure of the Cr_2O_3 film is controlled by the electroreduction rates of volatile Cr(VI) species, the electronic conductivity of the Cr_2O_3 film, and the re-volatilization of solid Cr_2O_3 in the presence of oxygen gas. The combination of these factors produce Cr_2O_3 films that are thinner and more amorphous near the LSM film perimeter, where film growth rates are anticipated to be rapid, and thicker, more crystalline Cr_2O_3 films further away from the LSM film perimeter, where the driving force for reduction of volatile Cr(VI) species is lessened due to the large voltage drop across the Cr_2O_3 film.

On the LSM surface, only $(Cr, Mn)_3O_4$ spinel phases were observed, and then primarily only next to the LSM film perimeter. Cross-sectional analyses showed that, within the LSM film, all concentrations of Cr were found in the general vicinity of the buried LSM-YSZ interface. Interpretation of these results lead us to believe that, at 800°C, the LSM-YSZ-air TPB, and adjacent LSM zones, electrochemically react with volatile Cr(VI) species during cathodic polarization to form the $(Cr, Mn)_3O_4$ spinel phase. Assuming that solid Cr_2O_3 forms on all YSZ-air surfaces within the porous LSM film, and $(Cr, Mn)_3O_4$ spinel crystals form on all LSM-air surfaces in and around the LSM-YSZ-air TPB, the original TPB region would be extensively altered in terms of composition and structure. The result would be that the cathode's ability to reduce oxygen would be severely compromised.

Taken together, the observations presented above suggest that electrochemically driven reactions influence the types of Cr species found throughout the cathode chamber of an SOFC. As such, all electroactive surfaces throughout the porous LSM film, whether they are located on the LSM or YSZ surfaces, will react with volatile Cr(VI) species. Even beyond the clearly identified LSM-YSZ-air and Cr_2O_3-YSZ-air electroactive interfaces, electrochemically influenced reactions, such as the formation of the $(Cr, Mn)_3O_4$ spinel phase, continue to occur, suggesting that removal of electrogenerated O^{2-} anions can occur well outside of the region traditionally viewed as the LSM-YSZ-air TPB.

Acknowledgments

The authors are grateful to the National Research Council/Natural Science and Engineering Research Council of Canada (NRC/NSERC) Research Partnership Program and Fuel Cell Energy, Inc. for the financial support of this work. We also thank Tony Wood and Tahir Joia of Fuel Cell Energy, Inc. for useful discussions and the provision of materials, Jon McGovern and Rick Humphrey at the University of Calgary Microscopy and Imaging Facility for SEM analyses, and Dr. Rob Marr at the University of Calgary Laboratory for Electron Microbeam Analysis (UCLEMA) for assistance with the electron microprobe analyses.

The University of Calgary assisted in meeting the publication costs of this article.

References

1. S. P. Jiang, *Solid State Ionics*, **146(1-2)**, 1 (2002).
2. S. P. Jiang, J. P. Zhang, and X. G. Zheng, *J. Eur. Ceram. Soc.*, **22**, 361 (2002).
3. S. P. Jiang, *J. Appl. Electrochem.*, **31**, 181 (2001).
4. Y. Matsuzaki and I. Yasuda, *J. Electrochem. Soc.*, **148**, A126 (2001).
5. Y. Matsuzaki and I. Yasuda, *Solid State Ionics*, **132**, 271 (2000).
6. S. P. Jiang, J. P. Zhang, L. Apateanu, and K. Foger, *J. Electrochem. Soc.*, **147**, 4013 (2000).
7. S. P. Jiang, J. P. Zhang, and K. Foger, *J. Electrochem. Soc.*, **147**, 3195 (2000).
8. S. P. Jiang, J. P. Zhang, and K. Foger, *J. Electrochem. Soc.*, **148**, C447 (2001).
9. Y. Larring and T. Norby, *J. Electrochem. Soc.*, **147**, 3251 (2000).
10. S. P. Jiang, J. P. Zhang, L. Apateanu, and K. Foger, *Electrochem. Commun.*, **1**, 394 (1999).
11. S. P. S. Badwal, R. Deller, K. Foger, Y. Ramprakash, and J. P. Zhang, *Solid State Ionics*, **99**, 297 (1997).
12. S. Taniguchi, M. Kadowaki, H. Kawamura, T. Yasuo, Y. Akiyama, Y. Miyake, and T. Saitoh, *J. Power Sources*, **55**, 73 (1995).
13. K. Hilpert, D. Das, M. Miller, D. H. Peck, and R. Weib, *J. Electrochem. Soc.*, **143**, 3642 (1996).
14. B. Borglum and E. Neary, Paper presented at the 2003 Fuel Cell Seminar Conference, Miami Beach, FL, Nov 3-7, 2003.
15. To be published.
16. D. H. Speidel and A. Muan, *J. Am. Ceram. Soc.*, **46**, 577 (1963).
17. E. Pollert, M. Nevriva, and J. Novak, *Mater. Res. Bull.*, **15**, 1453 (1980).
18. B. B. Ebbinghaus, *Combust. Flame*, **93**, 119 (1993).
19. P. Kofstad, *Nonstoichiometry, Diffusion, and Electrical Conductivity in Binary Metal Oxides*, p. 204, Wiley-Interscience, New York (1972)
20. I. Voigt and A. Feltz, *Solid State Ionics*, **63-65**, 31 (1993).

21. D. Waller, J. D. Sirman, and J. A. Kilner, in *Solid Oxide Fuel Cells V*, U. Stimming, S. C. Singhal, H. Tagawa, and W. Lehnert, Editors, PV 97-40, p. 1140, The Electrochemical Society Proceedings Series, Pennington, NJ (1997).
22. T. Horita, K. Yamaju, N. Sakai, Y. Xiong, H. Yokokawa, and T. Kawada, *Ionics*, **8(1/2)**, 108 (2002).
23. F. H. van Heuveln, H. J. M. Bouwmeester, and F. P. F. van Berkel, *J. Electrochem. Soc.*, **144**, 126 (1997).
24. J. Fleig, *J. Power Sources*, **105**, 228 (2002).